ORIGINAL ARTICLE

Journal
of the American Ceramic Society

The effect of imprint on remanent piezoelectric properties and ferroelectric aging of PbZr$_{0.52}$Ti$_{0.48}$O$_3$ thin films

Betul Akkopru-Akgun[1,2] iD | Wanlin Zhu[2] | Michael T. Lanagan[1,3] |
Susan Trolier-McKinstry[1,2] iD

[1]Center for Dielectrics and Piezoelectrics, Materials Research Institute, The Pennsylvania State University, University Park, Pennsylvania

[2]Department of Materials Science and Engineering, The Pennsylvania State University, University Park, Pennsylvania

[3]Department of Engineering Science and Mechanics, The Pennsylvania State University, University Park, Pennsylvania

Correspondence
Susan Trolier-McKinstry, Penn State University, University Park, Pennsylvania.
Email: set1@psu.edu

Funding information
National Science Foundation, Grant/Award Number: IIP-1361571 and 1361503

Abstract

Ferroelectric films suffer from both aging and degradation under high ac-field drive conditions due to loss of polarization with time. In this study, the roles of defect chemistry and internal electric fields on the long-term stability of the properties of piezoelectric films were explored. For this purpose, lead zirconate titanate (PZT) films with a Zr/Ti ratio of 52/48 doped with Mn- (PMZT) or Nb- (PNZT) were deposited on Pt coated Si substrates by the sol-gel method. It was demonstrated that the magnitude of the internal field is much higher in PMZT films compared to PNZT films after poling in the temperature range of 25-200°C under an electric field of -240 kV/cm. The development of the internal field is thermally activated, with activation energies from 0.5 ± 0.06 to 0.8 ± 0.1 eV in Mn doped films and from 0.8 ± 0.1 to 1.2 ± 0.2 eV in Nb doped films. The different activation energies for imprint suggests that the physical mechanism underlying the evolution of the internal field in PMZT and PNZT films differs; the enhanced internal field upon poling is attributed to (a) alignment of oxygen vacancy—acceptor ion defect dipoles (($Mn''_{Ti} - V^{\bullet\bullet}_O)^x$, ($Mn'_{Ti} - V^{\bullet\bullet}_O)'$) in PMZT films, and (b) thermionic injection of electron charges and charge trapping in PNZT films. In either case, the internal field reduces back switching, enhances the remanent piezoelectric properties, and dramatically improves the aging behavior. PMZT films exhibited the greatest enhancement, with reduced high temperature (180°C) aging rates of 2%-3%/decade due to improved stability of the poled state. In contrast, PNZT films showed significantly larger high temperature aging rates (15.5%/decade) in the piezoelectric coefficient, demonstrating that the fully poled state was not retained with time.

KEYWORDS
acceptor, aging, donor, imprint, PZT, sol-gel, thin film

1 | INTRODUCTION

Ferroelectric thin films are finding increased usage in a wide variety of microelectromechanical (MEMS) devices, including ink jet printers, adjustable optics, ultrasound transducers, resonators, energy harvesters, etc. Significant work has been done on deposition techniques and device fabrication technology over the last two decades[1–5]; however, there are comparatively few reports on long-term ferroelectric aging of these materials.[6–8] Thus, an understanding of the fundamental materials science that underpins the stability of the properties is lacking.

Aging in ferroelectric ceramics can be defined as the change of piezoelectric and dielectric properties with time, under zero external stress and isothermal conditions.[6] It originates from stabilization of the local domain structure and immobilization of domain walls, both of which reduce the extrinsic contributions to properties over time.[9] There are four principal mechanisms that restrict domain wall motion and change the local domain configuration, and consequently cause aging. These are: (a) migration of impurities and vacancies to domain walls to lower the wall energy (domain wall immobilization),[10] (b) accumulation of charge at grain boundaries; the resulting internal field stabilizes the polarization direction, (an interface effect)[11] (c) alignment of defects to decrease the dipolar energy (volume or bulk effect),[12] and (d) ferroelastic switching from a poled state to relieve local strains. In bulk ceramics, aging is often dominated by rearrangement of charged defects that stabilize the domain configuration through an electric or elastic field. This results in a decrease in the dielectric and piezoelectric properties over time.[10–15] The short-range motion of charged point defects (mainly oxygen vacancies), contributes to the reorientation of defect dipoles, while long-range motion of mobile ionic or electronic carriers results in formation of a space charge layer.[13,14] Therefore, aging and degradation of ferroelectric ceramics is intimately related to conduction.

Since the discovery of aging in bulk ferroelectrics in the 1950s,[9] significant effort has been spent on investigating the mechanisms for aging and their dependence on the concentration and type of defects and the associated charge transport mechanism.[6,14,16–19] In general, the defect chemistry is a function of oxygen partial pressure, temperature, and doping.[20] In particular, the dopant type and concentration play important roles in the aging rate. It is well known that oxygen vacancies help immobilize domain walls. Hard dopants like Fe or Mn in lead zirconate titanate (PZT) generate oxygen vacancies, which act to stabilize domain walls through mechanisms such as direct pinning of the wall and/or development of a preferred polarization direction. This will increase the aging rate.[21–23] Soft doping with niobium, on the other hand, lowers the aging rate relative to acceptor-doped and undoped PZT.[24]

The enhancement of domain wall mobility in soft materials has been explained in several ways: (a) reduction in space charge accumulation at domain walls (eg donor doping also decreases the hole concentration) (b) donor dopants compensate acceptor ions which are naturally present in the material and thus minimize the adverse effect of acceptor ions on aging, (c) compensation of lead vacancies by donor ions reduces the internal stress in the material so that domain walls becomes more mobile.[13,25] In mixed dopant systems, where both acceptors and donors are introduced, the relative and total concentrations of dopants determine the dominant aging mechanism. The presence of acceptor ions even at small

concentrations in highly donor doped PZT ceramics generates localized oxygen vacancies that act to increase aging rate.[26]

To diminish aging in ferroelectric thin films, a mechanism that restricts depolarization is required, eg by creating a preferred polarization state. This is known as imprint and is characterized by a shift in the polarization-electric field (P-E) hysteresis loop along the field axis.[7] There are two commonly used methods to introduce imprint in PZT thin films: (a) hot poling,[27] and (b) poling while illuminating under UV radiation.[27] The first method uses thermal energy to align defect dipoles along the polarization direction while the second method utilizes UV radiation to develop or redistribute space charge layers.[28–30] Both mechanisms generate internal electrical fields, leading to stabilization of the domain configuration along the polarization direction.

Different mechanisms have been proposed to explain imprint in PZT films; (a) the bulk screening model,[28] (b) the interface screening model,[31] and (c) the defect-dipole alignment model.[31] The bulk and interface screening models both assume the presence of a thin layer at the interface between the electrode and ferroelectric where the spontaneous polarization is suppressed and electronic charges are trapped.[31] In the bulk screening model, imprint is ascribed to the depolarizing field due to incomplete screening associated with the presence of a non-ferroelectric layer between the electrode and ferroelectric film.[32] In the interface screening model, on the other hand, an electrical field arises in the interfacial layer to compensate the depolarization field, leading to either charge injection from the electrode into the bulk of the film or charge separation within the interfacial layer.[31] Although both models have been successful in describing the UV-induced imprint phenomena in PZT films, only the interface screening can be reasonably used to describe the imprint behavior in hot-poled ferroelectric films.[31]

In contrast, imprint in ferroelectric films due to defect-dipole alignment in a poling field associated with oxygen vacancy migration around acceptor ions.[31,33] Introducing acceptor ions increases the vacancy concentration while addition of donors favors negatively charged cation vacancies. Since the oxygen vacancy concentration decreases after donor doping, an enhancement in the internal field is expected after doping with acceptor, rather than donor ions.[34]

Since imprint in PZT films is linked in at least some cases to defect-dipole alignment, the effect of doping on imprint is crucial to understanding the link between imprint and aging. The objective of this study is to understand how defect chemistry and internal electric fields develop in piezoelectric films, as well as the effect of these parameters on the long-term stability of the properties. For this purpose, Mn and Nb doped $PbZr_{0.52}Ti_{0.48}O_3$ thin films were deposited on platinized Si substrate using spin coating of a sol-gel solution. All samples were characterized by X-ray diffraction and field emission scanning electron microscopy to ensure that no second phases develop. Then, the ferroelectric and

dielectric properties were examined before and after poling at 25-200°C. The poling conditions (poling time, magnitude of the electric field, and temperature) were used to modulate the remanent polarization and the degree of imprint developed.[8,35] High temperature aging at 180°C was performed to investigate the stability of the developed imprint and the functional properties of the films.

2 | PREPARATION OF MN AND NB DOPED PZT THIN FILMS

2.1 | Sol preparation

Two series of PZT thin film solutions with Mn and Nb doping levels from 0.5-4 mol.% were prepared from lead acetate trihydrate (Pb(CH$_3$·CO$_2$)$_2$·3H$_2$O, Sigma-Aldrich, St. Louis, MO), zirconium (IV) propoxide (Zr(OCH$_2$CH$_2$CH$_3$)$_4$, Sigma-Aldrich), titanium (IV) isopropoxide (Ti(OCH(CH$_3$)$_2$)$_4$, Sigma-Aldrich), manganese (II) acetate tetrahydrate ((CH$_3$COO)$_2$Mn·4H$_2$O, Sigma-Aldrich) and niobium (V) ethoxide (Nb(OCH$_2$CH$_3$)$_5$, Sigma-Aldrich), 2-methoxyethanol (CH$_3$OCH$_2$CH$_2$OH, Sigma-Aldrich), acetylacetone (CH$_3$COCH$_2$COCH$_3$, Sigma-Aldrich) and acetic acid (CH$_3$CO$_2$H, Sigma-Aldrich). Solutions with a Zr/Ti ratio of 52/48 were prepared using 10 mol% Pb excess to compensate for lead loss during heat treatment. The preparation of precursor solutions is similar to that described elsewhere.[36]

For preparation of Mn doped PZT films, 20 g of lead acetate trihydrate and 0.058-0.47 g of manganese acetate were dissolved in 120 mL of 2-methoxyethanol (2-MOE) under Ar in a rotary evaporator flask placed in an oil bath at 120°C. The solution was then dehydrated under vacuum until complete precipitation occurred. In a separate beaker, 11.2 g of zirconium n-propoxide and 6.48 g of titanium isopropoxide were dissolved in 150 mL of 2-MOE and stirred for 30 min in a glove box. The resultant solution was slowly added into the Pb/Mn powders in the heated flask; the entire solution was refluxed for 2 hours under Ar at 120°C. Following refluxing, the solution was vacuum distilled and then diluted with 2-MOE (5 vol %) and acetylacetone (22.5 vol %) to achieve the desired solution molarity of 0.40 mol/L. The Mn doping concentration in solution was calculated as Pb$_{(1.1-(1/2)x)}$Zr$_{0.52(1-x)}$Ti$_{0.48(1-x)}$Mn$_x$O$_{3.1}$, $x = 0.005-0.04$.

The processing of Nb doped PZT solutions is very similar to that used for Mn doped PZT films. The only difference is that the Nb(OC$_2$H$_5$)$_5$ was added to the Ti/Zr/2-MOE solution and stirred for 30 minutes in the glove box. The solution composition was batched as Pb$_{(1.1-(1/2)x)}$Zr$_{0.52(1-x)}$Ti$_{0.48(1-x)}$Nb$_x$O$_{3.1}$, where $x = 0.005-0.04$. Subsequent steps were identical to those used in the processing of Mn doped PZT thin films, where the Zr/Ti/Nb solution was added to he Pb-containing powder and refluxed at 120°C to obtain the final solution.

2.2 | Coating process

Silicon substrates with a thick thermal SiO$_2$ barrier layer, 200Å of Ti and 1500Å of Pt (Nova Electronic Materials, Inc., Richardson, TX) were used in this study. Prior to coating, the substrates were exposed to rapid thermal processing at 500°C for 60 seconds to remove surface moisture. Doped PZT films were prepared via spin coating. First, the solution was dispensed onto the substrate through a 0.1 μm polytetrafluoroethylene (PTFE, Restek) syringe filter. Then a single layer was spun at 1500 rpm for 30 seconds. Each layer underwent two pyrolysis treatments for 3 minutes at 250 and 450°C, respectively. The film was then crystallized at 700°C for 60 seconds by rapid thermal annealing (RTA). The process was repeated six times until a desired thickness of nearly 0.4 μm was built up. Finally, a single PbO layer was coated onto the surface of PZT films and then heat treated at 700°C in air, to remove surface pyrochlore. Residual PbO was then removed by immersing the sample in a 4 mol/L acetic acid solution for 60 seconds.

3 | MATERIALS CHARACTERIZATION

Glancing Incidence X-ray Diffraction (GIXRD) was performed to examine the structural and orientation of the films using an X'Pert Pro MPD diffractometer (PANalytical, Almelo, The Netherlands). The x-ray source was Cu $K\alpha$ radiation, with an accelerating voltage of 40 kV. The step size and hold time at each step was 0.02° and 10 seconds, respectively. X-ray diffraction patterns were recorded between 10° and 80° 2θ.

The coating morphology was examined using a Leo 1530 model field emission scanning electron microscope (FESEM) (LEO Electron Microscopy Ltd., Cambridge, UK) operated at 5 kV. Surface images were obtained in secondary electron imaging mode. The film thickness was measured using an Alpha-Step 500 Surface Profilometer (Tencor, Portsmouth, NH).

For electrical characterization, Pt top electrodes with diameters ranging from 200 μm to 1 mm were prepared by double layer photolithography and lift off processing. For this purpose, ~100 nm thick Pt films were sputter deposited on the PZT surface (CMS-18 Sputter System, Kurt J. Lesker Company, Pittsburgh, PA). After liftoff, the patterned Pt top electrodes were postannealed at temperatures in the range of 500 to 750°C. The bottom Pt electrode was exposed using buffered HF to etch the PZT layers. The low field dielectric properties of the PZT films were determined using an LCR meter (Hewlett-Packard 4284A Precision, Agilent Technologies, Inc., Palo Alto, CA). All measurements were performed at 1 kHz with an oscillation voltage of 0.03 V. Hysteresis measurements were made using a Precision Multiferroic Analyzer (Radiant Technologies, Inc., Albuquerque, NM) using a triangular waveform and

a frequency of 100 Hz. The longitudinal piezoelectric co-efficient ($d_{33,f}$) of the PZT films was determined by double beam laser interferometry (AixACCT DBLI). Prior to measurements, the samples were first poled at temperatures from 25 to 200°C using an HP 6200B dc power supply (Agilent Technology) with a DC electrical field five times higher than the coercive field for 30 minutes.

The first order reversal curves method (FORC) was used to determine the reversible and irreversible FORC distributions.[37] First order reversal curves were taken using a homemade polarization measurement system with voltage amplifiers (BOP 1000M, Kepco and TREK 609C-6, Piezotronics Inc., Depew, NY). The films were initially pre-poled under an electric field of −240 kV/cm at 25 and 150°C for 30 minutes. Then, a family of P-E hysteresis loops (40 different loops) was recorded using an electric field cycle from a negative saturation field $−E_{max}$ to a field α_i where α_i changes from $−E_{max}$ to $+E_{max}$. The instantaneous descending electric field was β_i, The polarization was measured for α_i from $−E_{max} + n\Delta E$, n = 2 to 40 and β_i, from $−E_{max} + k\Delta E$, k = 0, 1, 2, …, n, respectively. The irreversible and reversible FORC distributions are defined for ($\alpha_i \in \alpha$) and ($\beta_i \in \beta$) as:[38]

$$p(\alpha,\beta) = \frac{1}{2} \frac{\partial^2 P(\alpha,\beta)}{\partial\alpha\partial\beta} \quad (1)$$

$$p_{rev}(\alpha) = \lim_{\beta\to\alpha-} \frac{1}{2} \frac{\partial P(\alpha,\beta)}{\partial\beta} \quad (2)$$

where α and β are the up- and down-switching fields of some population of hysterons, respectively. For $\alpha > \beta$, the hysterons are irreversible and for $\alpha = \beta$, the hysterons are reversible.

3.1 | Aging measurements

Before the aging test, samples were poled at 150°C under an electric field of 240 kV/cm for 30 minutes. Then, the samples were aged at zero field under closed circuit conditions at 180°C. High temperatures were used to accelerate the aging process. The piezoelectric response, $d_{33,f}$, was then measured at room temperature as a function of the time spent aging at elevated temperature. The time variation of $d_{33,f}$ follows a well-known logarithmic law. The percent change of piezoelectric response (d_{33}) per decade
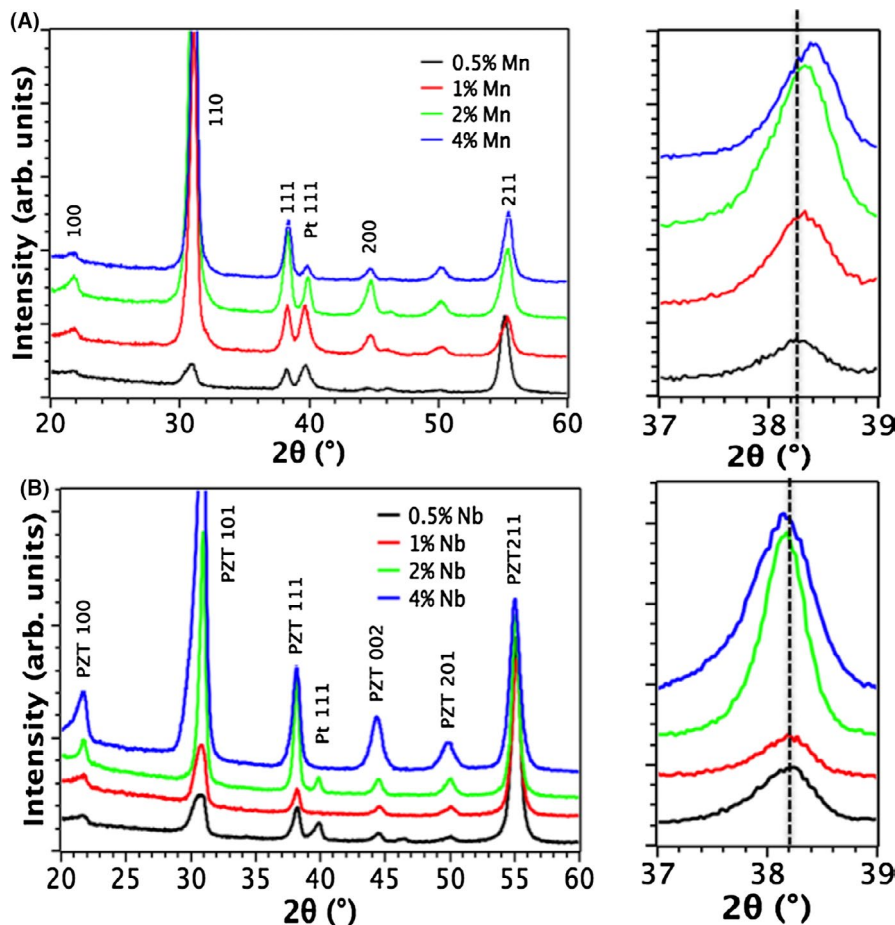

FIGURE 1 Glancing angle XRD diffraction patterns of (A) Mn and (B) Nb doped PZT thin films [Colour figure can be viewed at wileyonlinelibrary.com]
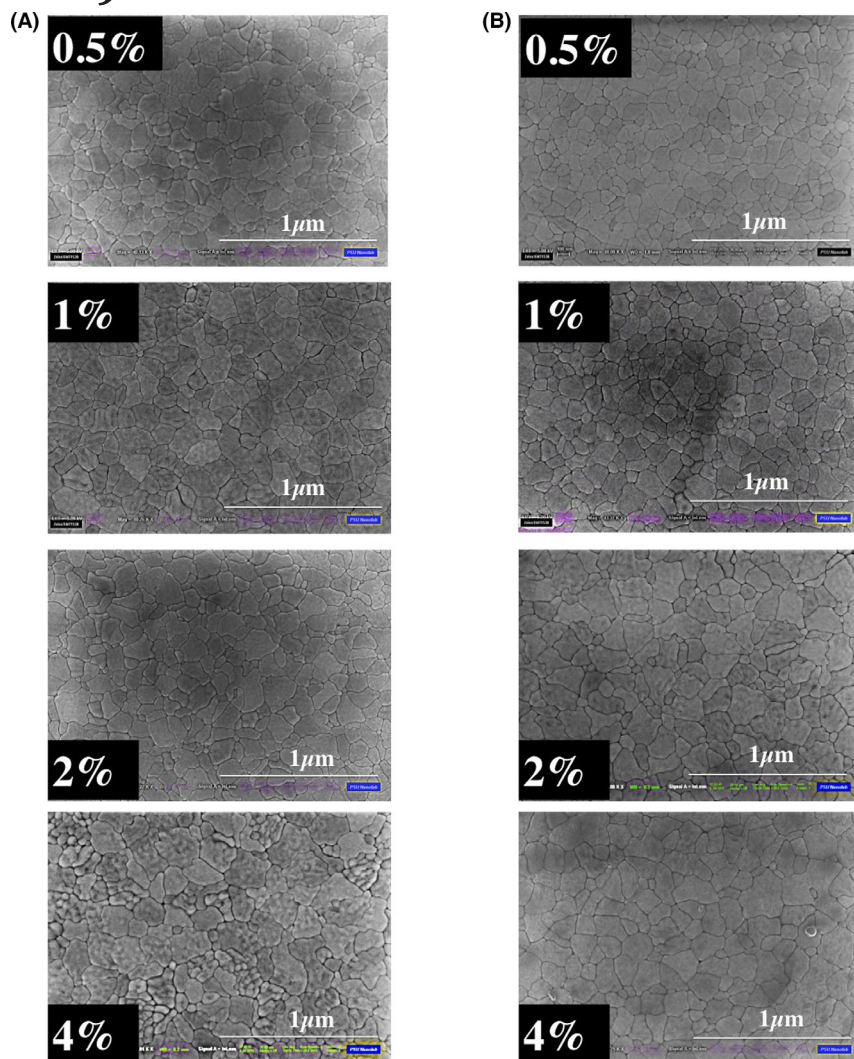
FIGURE 2 Top surface FESEM images of (A) Mn, and (B) Nb doped PZT films [Colour figure can be viewed at wileyonlinelibrary.com]

of time (eg one order of magnitude change) was calculated using the following relationship with time.

$$d_{33,f}(t) = d_{33,f}(t_0) - r\log(t) \quad (3)$$

where $d_{33,f}(t)$ is the longitudinal piezoelectric coefficient measured after an aging time t, $d_{33,f}(t_0)$ is longitudinal piezoelectric coefficient at t_0, $(t_0 < t)$, and r is the rate of decay. Similarly, P-E hysteresis measurements were conducted following different aging times to monitor the change in the magnitude of imprint for the PMZT and PNZT films."

4 | RESULTS AND DISCUSSION

4.1 | Phase identification and microstructure of PZT thin films

The surface morphology and structure of Mn and Nb doped PZT films after annealing at 700°C in O_2 were studied by FESEM and GIXRD. Figure 1 shows that all films have the perovskite structure.[37] No peaks corresponding to secondary phases such as excess PbO or pyrochlore were observed in the XRD patterns, suggesting that at most trace amounts of

secondary phases exist in either set. As shown in Figure 1, the films with low Mn and Nb concentrations are approximately randomly oriented. With increasing Mn concentration, XRD peaks shifted toward higher angles, indicating decreased out-of-plane lattice parameters for the PMZT films. The results for the Mn doped film are comparable to those reported by Zhu et al.[39] The same group reported no change in lattice parameter with Nb doping.[40]

Figure 2 exhibits FESEM surface micrographs of the Mn and Nb doped PZT films grown on Pt/Ti/SiO$_2$/Si substrates. As shown there, both Mn and Nb doped PZT films were smooth, homogeneous and of high density; no crack formation was observed. SEM results confirmed that the grain size in both Mn and Nb doped PZT films is similar and varies between 30-150 nm.

4.2 | Thermal imprint in Mn and Nb doped PZT films

The high field dielectric response of 1% Mn and 1% Nb doped PZT films before and after poling at 25 and 150°C for 30 minutes was analyzed using the irreversible FORC
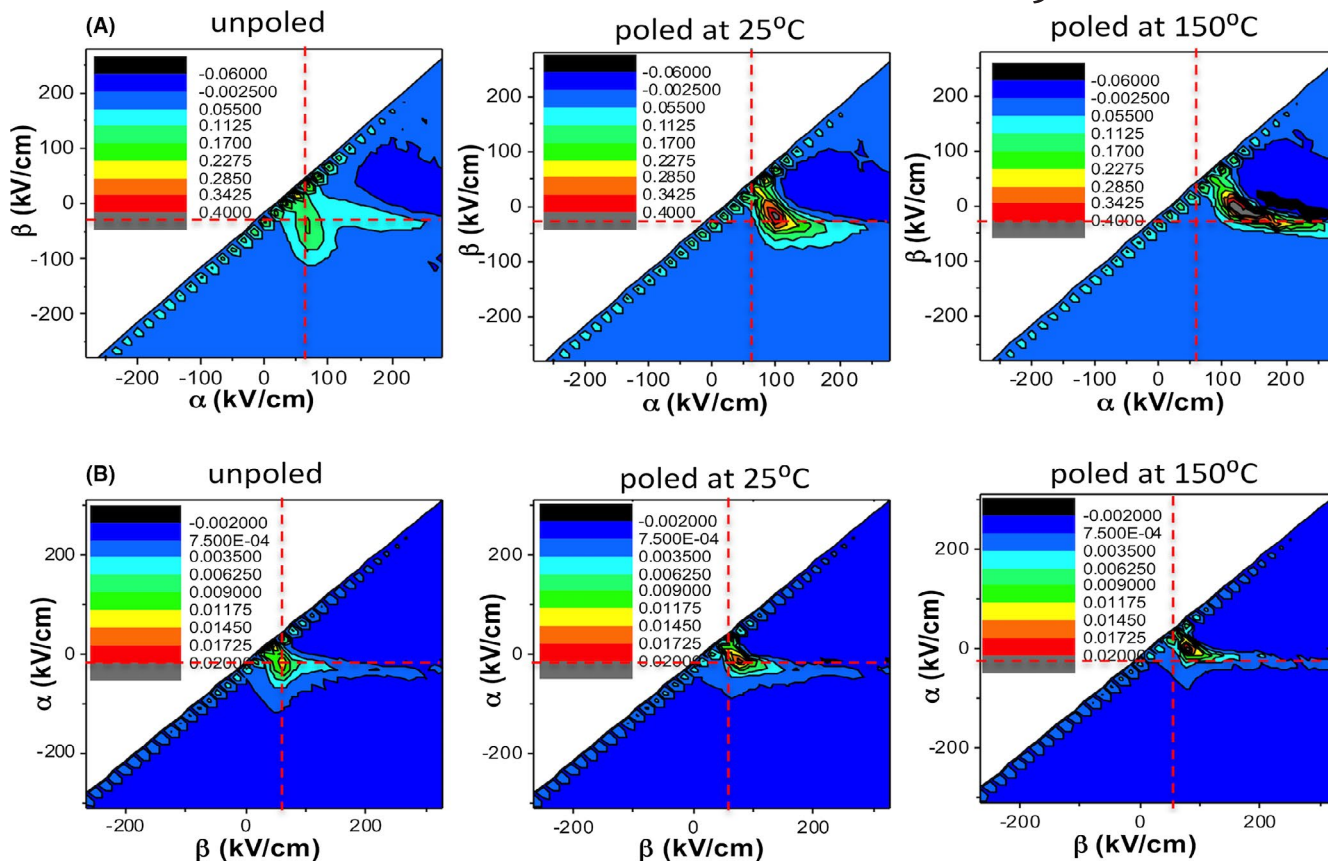
FIGURE 3 The irreversible FORC distributions of the (A) 1% Mn and (B) 1% Nb doped PZT films before and after poling at 25 and 150°C [Colour figure can be viewed at wileyonlinelibrary.com]

distributions, where α and β are the up- and down-switching fields of some population of hysterons, respectively, as shown in Figure 3. The appearance of periodic features along the $\alpha = \beta$ line of Figure 3 is an artifact arising from the algorithm used for calculation. In unpoled Mn doped PZT films, the irreversible FORC distribution was broadened, which means that up and down switching fields for the hysterons show more variability. It is probable that this is a result of the fact that incorporation of Mn into PZT generates defect dipoles, which change the local electric/elastic field, modulating the switching of the hysterons. Since Nb doped PZT films have a low concentration of defect dipoles involving oxygen vacancies, the FORC distribution is very sharp. After poling, the distribution of switching fields becomes sharper for both Mn and Nb doped films. Additionally, the up- and down-switching fields for the hysterons shifts further from the $\alpha = -\beta$ line, consistent with the development of imprint. This shift is more noticeable in Mn doped PZT films, compared to their Nb doped counterparts, indicating a higher magnitude of imprint in PMZT films. Mn doped PZT films have higher concentration of defect dipoles (acceptor ions and oxygen vacancies) that can be aligned along the polarization direction during poling to introduce imprint.[7]

Figure 4 shows the effect of imprint on the reversible FORC distributions. It is seen that poling of both Mn and Nb doped films shifts the reversible FORC distributions along the field axis, another indication of imprint in the PZT films. The degree of imprint was enhanced as the poling temperature increased. For PMZT films, the internal field is 14 and 28 kV/cm after poling at 25 or 150°C, respectively. For PNZT films, on the other hand, the magnitude of internal field was smaller; it is 7 kV/cm after poling at 25°C and it increased to 14 kV/cm after poling at 150°C. Furthermore, the maximum in the reversible FORC distribution increases after poling; this is most noticeable in Mn doped PZT films after hot poling. This increase is presumably related to the restoring force provided by the imprint field. The restoring force tends to align domains perturbed by the electric field, making the response more reversible and increasing the intensity of the reversible FORC distribution.

The effect of thermal imprint on the ferroelectric properties of Mn and Nb doped films was also investigated by P-E hysteresis measurements; the findings are in agreement with the FORC results. Figure 5 shows the hysteresis loops of unpoled and poled PZT thin films doped with 1 mol.% Nb or Mn, measured up to 400 kV/cm. As shown in Figure 5,
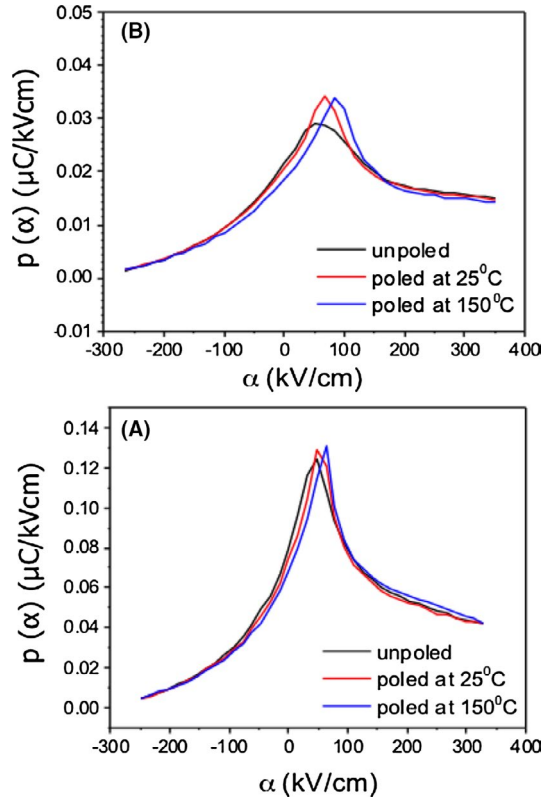
FIGURE 4 Reversible FORC distributions of (A) 1% Mn doped and (B) 1% Nb doped PZT films [Colour figure can be viewed at wileyonlinelibrary.com]

FIGURE 5 Variation in the P-E hysteresis loop of (A) 1% Mn and (B) 1% Nb doped PZT films after poling at different temperatures [Colour figure can be viewed at wileyonlinelibrary.com]

the hysteresis loops of both films move to positive voltages after poling at −240 kV/cm (such that the direction of poling field is pointed from the top to the bottom electrode). The shift becomes more noticeable as the poling temperature increases. It is apparent that films poled at room temperature under these conditions have nearly symmetrical hysteresis loops, as do films that were originally unpoled. However, as the poling temperature is increased to 200°C, a strong imprint progressively develops. This is manifested primarily as a left-right shift on the loop, without significant degradation in the switchable polarization (Figure 5). In the same way, there is no strong evidence for development of significant levels of leakage at either electrode following the high temperature poling.

Figure 6 exhibits the level of imprint in PMZT and PNZT films as a function of poling temperature. The magnitude of imprint was determined from the voltage shifts in P-E hysteresis loops. The internal field can be defined as,

$$E_i = \frac{+E_c - |-E_c|}{2} \quad (4)$$

where E_i is the internal field, $+E_c$ is the positive coercive field, and $-E_c$ is the negative coercive field. As shown in Figure 6, the response of PNZT and PMZT films to poling is considerably different. For PMZT and PNZT films, the internal fields
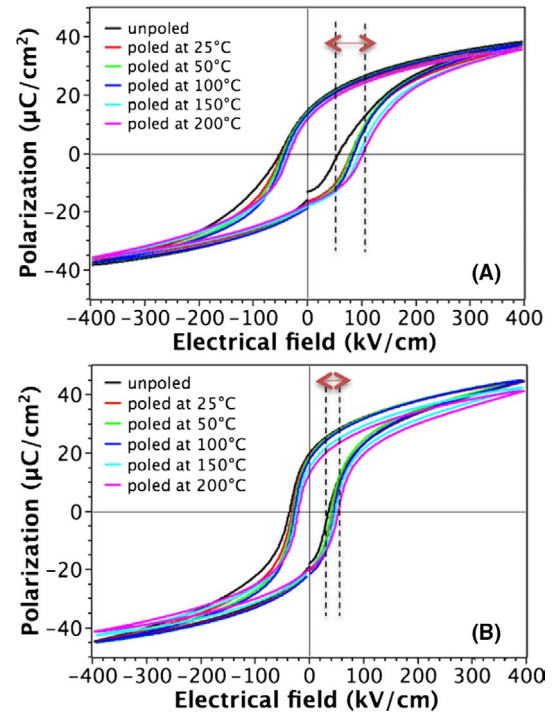
ranged from 3 to 32 kV/cm and 0.5 to 18 kV/cm, respectively. For all dopant levels and poling temperatures, the magnitude of imprint was higher in the PMZT films. The temperature dependence of the voltage shift in the P-E hysteresis was found to follow an Arrhenius type behavior for both donor and acceptor-doped PZT films. As shown in Figure 6B, the activation energies (E_a) extracted from the slopes of the Arrhenius plots for Mn doped PZT films ranged between 0.5 ± 0.06 and 0.8 ± 0.1 eV. These are much lower than E_a for their Nb doped counterparts (0.8 ± 0.1 to 1.2 ± 0.2 eV).

Addition of Mn on the perovskite Zr/Ti site in PZT can create defect dipoles such as $(Mn''_{Ti} - V^{··}_O)^x$, $(Mn'_{Ti} - V^{··}_O)'$ when it is ionically compensated by oxygen vacancies. Additionally, evaporation of PbO could, in principle, lead to formation of $(V''_{Pb} - V^{··}_O)^x$ defect associates. Oxygen vacancies are the most mobile ions in PZT and short-range migration of oxygen vacancies around the acceptor can generate an internal field in PZT films at poling temperatures and fields.[41,42] Presumably, the concentration of defect associates increases with Mn concentration in the PZT, enhancing the propensity of defect-dipole alignment upon thermal poling of PZT films. Indeed, the E_a for imprint in Mn doped PZT films varies between 0.5 and 0.8 eV, which is close to the activation energy required for migration of oxygen vacancies (Table 1).[43] This suggests that imprint in Mn doped PZT films is governed via defect-dipole alignment rather than injecting and/or trapping of electronic charges (Figure 10B). To further support this hypothesis, leakage current
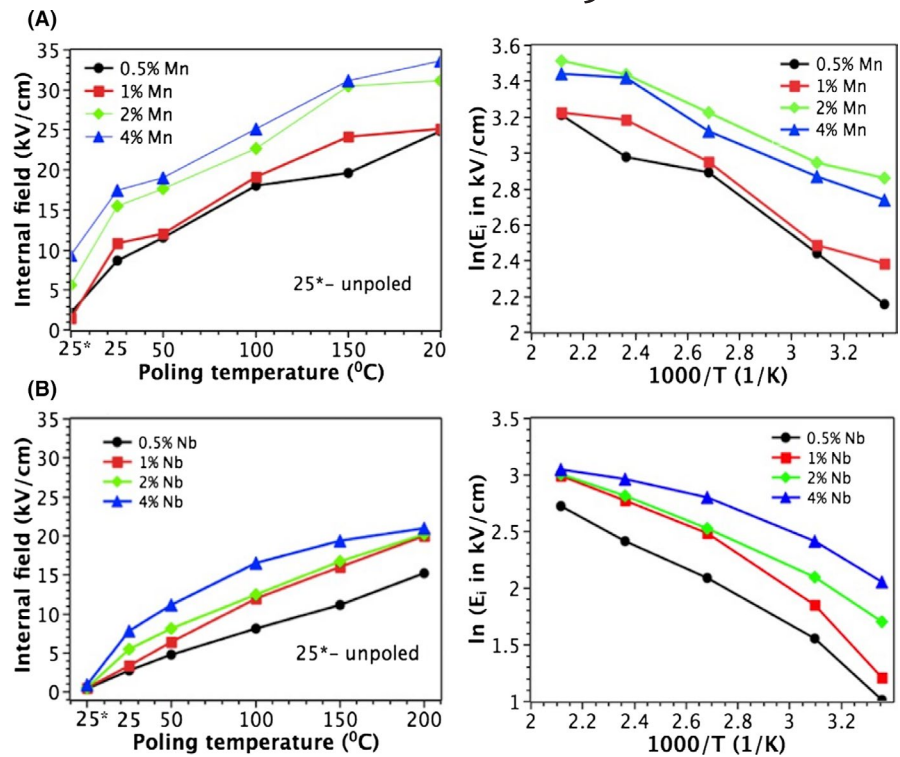
FIGURE 6 Magnitude of the internal field in (A) Mn and (B) Nb doped PZT films determined from P-E loops measured after poling at different temperatures. Activation energies for internal field were calculated from the slope of the graphs [Colour figure can be viewed at wileyonlinelibrary.com]

measurements were conducted to explore the dominant conduction mechanism over the range of temperatures used for development of imprint in PMZT films (Figure 7). It was found that the leakage current is controlled via Schottky emission and potential barrier height for thermionic injection of electronic charges varies between 0.72 to 1.12 eV, which exceeds E_a for imprint in Mn doped PZT films (Table 2).

In contrast to Mn doped PZT films, the activation energy for imprint in Nb doped PZT films (0.8 ± 0.1 to 1.2 ± 0.2 eV) (Table 1) was much higher than the activation energy required for migration of oxygen vacancies (0.5-0.6 eV). It is intriguing that, particularly in the case of the lower Nb concentrations, the activation energy for imprint is comparable to the activation energy for failure of many undoped PZT films.[44] The higher activation energies for imprint in PNZT films suggest that defect-dipole alignment is not the only mechanism contributing to imprint. Indeed, the only source for generation of oxygen vacancies in Nb doped PZT films is evaporation of PbO upon annealing at temperatures higher than 450°C, which could lead to formation of $(V''_{Pb} - V^{..}_{O})^x$ dipoles. The oxygen vacancy concentration reduces with increasing Nb levels in PZT films, which would suppress the internal field originating from defect-dipole alignment upon thermal poling. However, it was found that the magnitude of imprint increases at higher Nb concentrations. This strongly suggests that defect-dipole alignment model alone cannot explain the magnitude of imprint observed in Nb doped PZT films.

It is possible that charge injection, the propensity for long-range migration of oxygen vacancies, or differences in the original film stoichiometry can also contribute to the

TABLE 1 Activation energies for imprint in PMZT and PNZT films

PMZT films	0.5% Mn	1% Mn	2% Mn	4% Mn
E_a (eV)	0.8 ± 0.1	0.7 ± 0.1	0.6 ± 0.1	0.5 ± 0.06
PNZT films	0.5% Nb	1% Nb	2% Nb	4% Nb
E_a (eV)	1.2 ± 0.2	1.2 ± 0.2	0.9 ± 0.1	0.8 ± 0.1

observed imprint.[31,45] To explore the contribution of electronic charges to the built in internal field, leakage current measurements were conducted on Nb doped PZT films. For lower Nb concentrations (0.5% and 1% Nb), the conduction is mainly controlled by Schottky emission in the temperature and electric field (240 kV/cm) range used to create an internal field in PZT films (Figure 8). It is intriguing that the potential barrier height for thermoionic emission of electrons from the electrode into the PNZT is approximately 1 eV (Table 2), which is comparable to the activation energy (1.2 ± 0.2 eV) for generation of imprint in PZT films. Furthermore, impedance measurements were conducted to explore defect sites at which injected electronic charges could be trapped. Figure 9 shows the temperature dependence of the modulus and conductivity for 1% Nb doped PZT films. The calculated activation energy for Nb doped PZT film is 1.1 ± 0.06 eV, which is attributed to electron trapping by Ti^{4+}.[22,25]

$$Ti^{4+} + e' \rightarrow Ti^{3+} \tag{5}$$
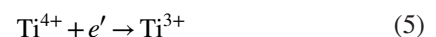
It is believed that imprint in 0.5 and 1% Nb doped PZT films results from electron injection from electrode into the
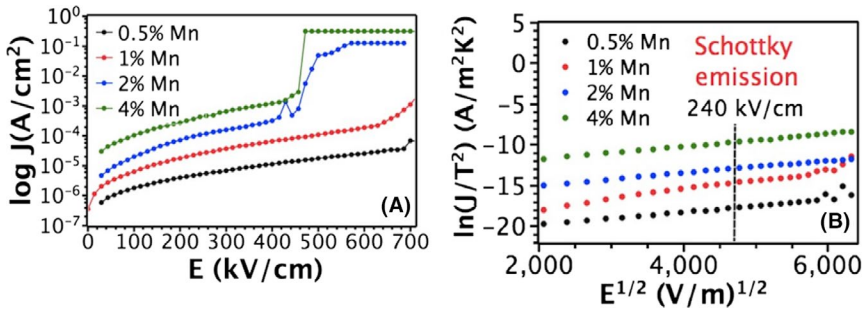
FIGURE 7 A, The variation of leakage current density with electric field in Mn doped PZT films; B, Fitting of the leakage current-voltage measurements over a range of temperature for Mn doped PZT thin films [Colour figure can be viewed at wileyonlinelibrary.com]

TABLE 2 Schottky barrier heights in PMZT and PNZT films

PMZT films	0.5% Mn	1% Mn	2% Mn	4% Mn
Φ_B (eV)	1.17 ± 0.04	1.06 ± 0.05	0.84 ± 0.03	0.72 ± 0.04
PNZT films	0.5% Nb	1% Nb	2% Nb	4% Nb
Φ_B (eV)	0.95 ± 0.05	1.07 ± 0.03	1.15 ± 0.04	1.24 ± 0.04
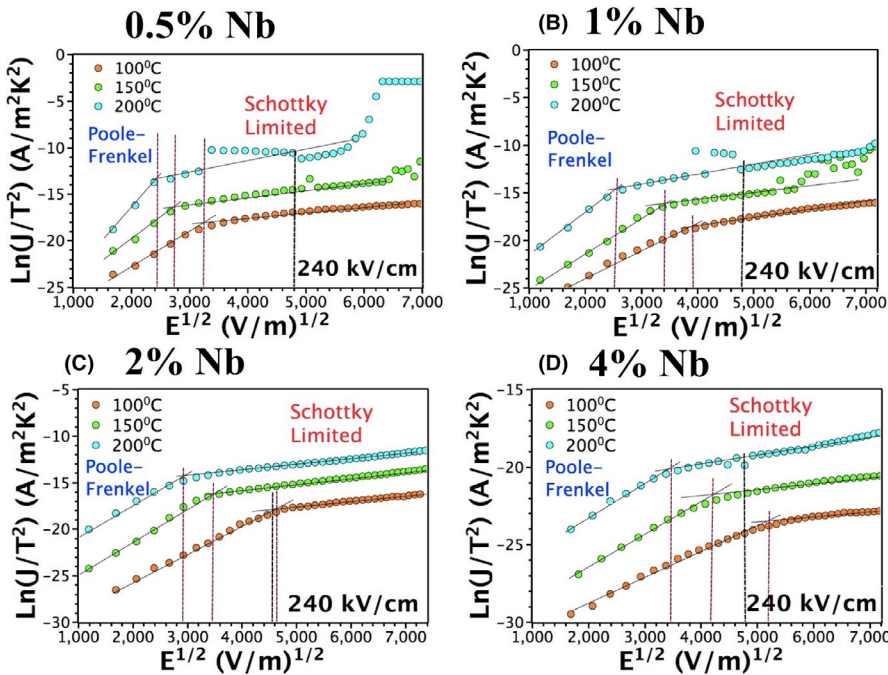
FIGURE 8 Fitting of the leakage current measurements over a range of temperature for (A) 0.5%, (B)1% Nb, (C) 2% Nb, and (D) 4% Nb doped PZT thin films [Colour figure can be viewed at wileyonlinelibrary.com]
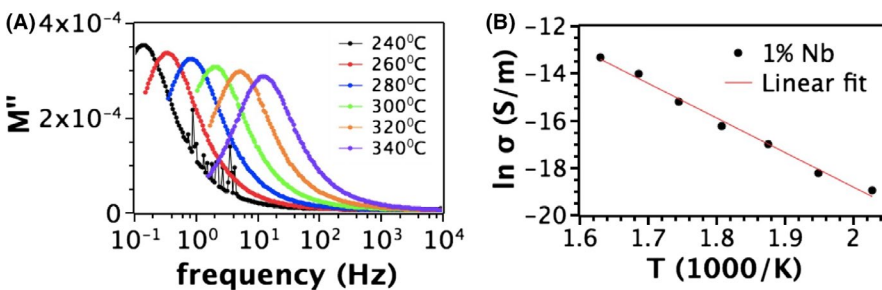

FIGURE 9 (A) Imaginary modulus of 1% Nb doped PZT film plotted as a function of frequency at different temperatures. (B) Change in conductivity of 1% Nb doped PZT films with temperature [Colour figure can be viewed at wileyonlinelibrary.com]

dielectric and subsequent electron trapping by Ti^{4+} sites (Figure 10A). With an increase in Nb concentration, Poole-Frenkel emission starts contributing to the electronic conduction below than 150°C, leading to a discrepancy between the imprint E_a (0.8-0.9 eV) and the calculated Schottky barrier height (1.15-1.24 eV).

It was found that the internal field has a significant effect on the remanent piezoelectric properties, such as the
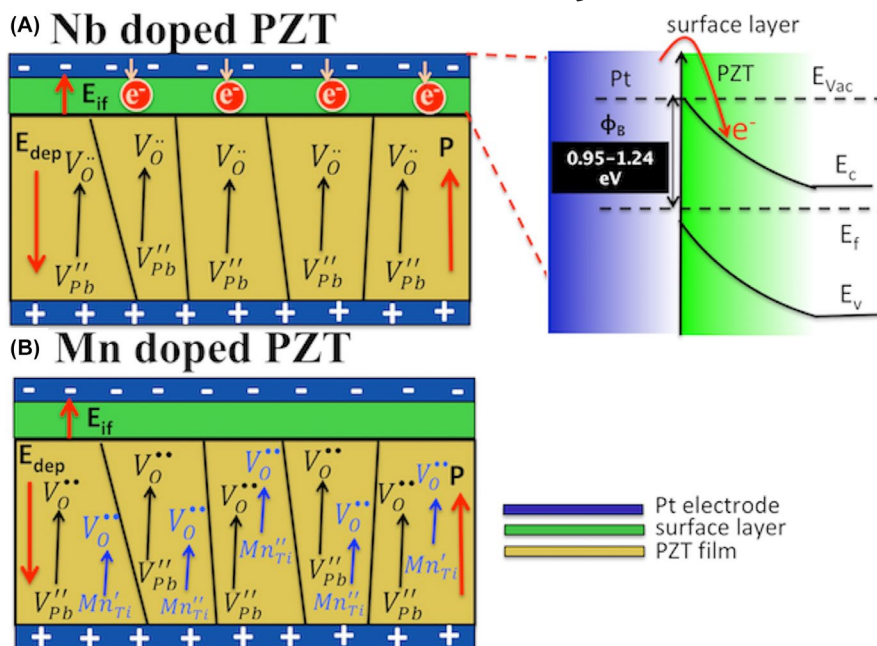
FIGURE 10 Schematic representations of the physical models for development of imprint in (A) Nb doped and (B) Mn doped PZT films [Colour figure can be viewed at wileyonlinelibrary.com]
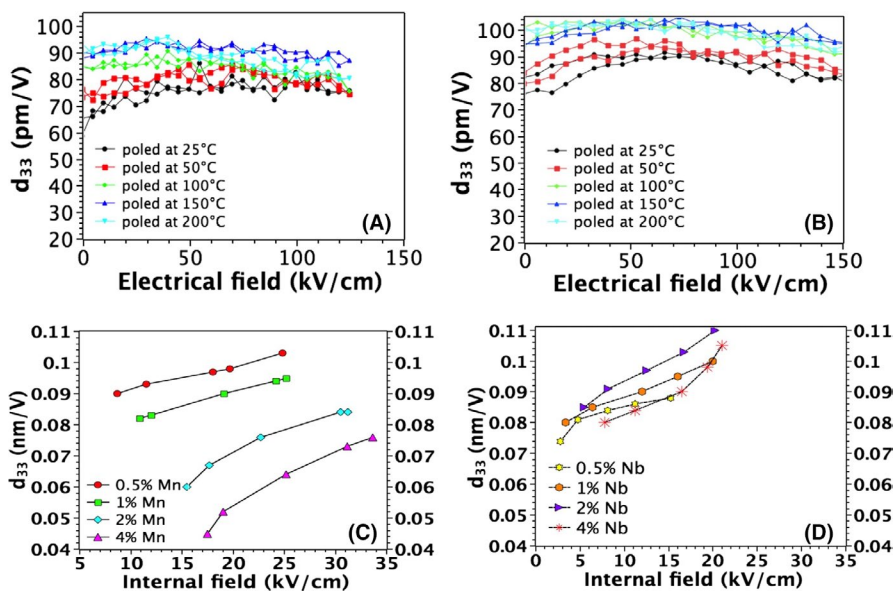

FIGURE 11 Variation of the magnitude of $d_{33,f}$ of (A) 1% Mn doped, (B) 1% Nb doped PZT films after poling at 25, 50, 100, 150, and 200°C, (C) 0.5, 1, 2, 4% Mn, (D) 0.5, 1, 2, 4% Nb doped PZT films after poling at 150°C [Colour figure can be viewed at wileyonlinelibrary.com]

longitudinal piezoelectric coefficient ($d_{33,f}$). Figure 11A,B show the longitudinal piezoelectric coefficients of 1% Mn and 1% Nb doped PZT films after poling at temperatures ranging from 25 to 200°C. The data were taken by driving the film with a unipolar field parallel to the poling direction to progressively higher electric fields in the range of 50-150 kV/cm. There are several key points that are apparent from these figures. First, the films that had been poled at room temperature or 50°C had relatively smaller remanent $d_{33,f}$ coefficients than those poled at higher temperatures. When driven to progressively higher electric fields (>50 kV/cm), the films repole, producing hysteretic responses. In contrast, films poled at higher temperatures showed larger remanent $d_{33,f}$ values,

and substantially less hysteresis in the instantaneous $d_{33,f}$ as a function of the drive field. This indicates that the net polarization in the PMZT and PNZT films poled at higher temperatures are more stable than the ones poled at room temperature. Secondly, the maximum value of the $d_{33,f}$ observed was larger for higher poling temperatures. For 1% Mn doped PZT film, the remanent $d_{33,f}$ value after poling at 25°C is 66 pm/V, increasing to 75 ± 2, 85 ± 2, 90 ± 2, and 92 ± 3 pm/V after poling the sample at 50, 100, 150, and 200°C. Similarly, the 1%Nb doped PZT film poled at 25°C has a remanent $d_{33,f}$ of 80 pm/V; the remanent $d_{33,f}$ increased to 84 ± 1, 92 ± 1, 96 ± 1, and 98 ± 2 pm/V after poling the sample at 50, 100, 150, and 200°C. These results are consistent with better
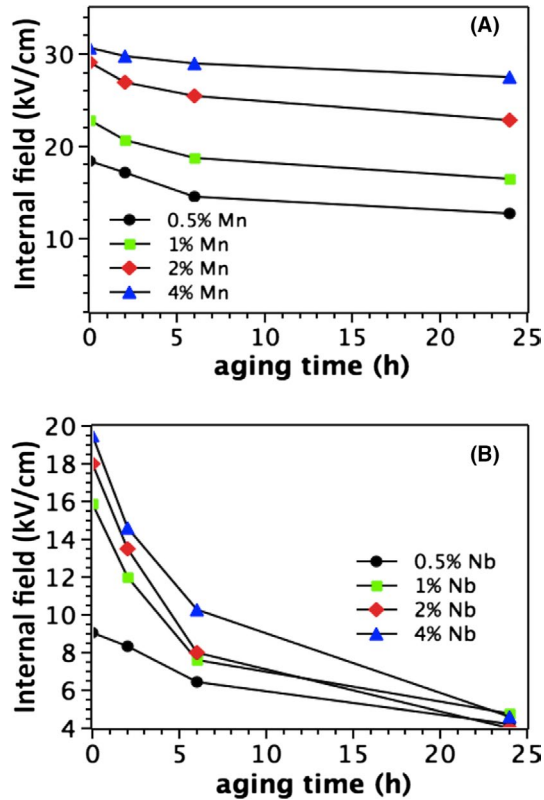
FIGURE 12 Time stability of imprint in (A) Mn and (B) Nb doped PZT films measured at room temperature after aging at 180°C [Colour figure can be viewed at wileyonlinelibrary.com]

alignment of the polarization along the electric field direction upon poling.[7]

Figure 11C,D exhibit the change in $d_{33,f}$ with internal field for PZT-based films with different Mn and Nb concentrations. It was observed that the internal field improves the $d_{33,f}$ for both PMZT and PNZT films. However, the enhancement in $d_{33,f}$ due to imprint is more obvious in PMZT films, where larger internal fields can be introduced (Figure 11). As shown in Figure 11C, the longitudinal piezoelectric coefficient of 4% Mn doped PZT films is almost doubled after poling at 200°C. For 4% Nb doped PZT films, on the other hand, $d_{33,f}$ only increased by ~30% relative to its 25°C-poled counterpart. The larger increase in $d_{33,f}$ after poling at high temperatures in Mn doped PZT films can be attributed to an enhanced internal field due to alignment of defect dipoles ($(Mn''_{Ti} - V_O^{\cdot\cdot})^x$, $(Mn'_{Ti} - V_O^{\cdot\cdot})'$) along the polarization direction during poling.

Another finding of Figure 11C,D is that for both Mn and Nb doped films, the internal field and corresponding $d_{33,f}$ increased with doping concentration. As reported in the literature, the alignment of oxygen vacancy and acceptor ion defect dipoles during poling introduces imprint in PZT ceramics.[46,47] When oxygen vacancies either move around an acceptor center to produce a defect dipole, or migrate long distances to produce space charge, it results in formation of

internal field in PZT films, which in turn enhances the piezoelectric properties. Since the oxygen vacancy concentration increases as higher concentrations of Mn are introduced into PZT films, an enhanced internal field and $d_{33,f}$ are expected. However, in the case of Nb doped PZT films, the increase in internal field and $d_{33,f}$ cannot be explained based on the defect-dipole alignment model since the oxygen vacancy concentration decreases after donor doping. It is believed that internal field in Nb doped PZT films results from both thermoionic emission of charges and Poole-Frenkel emission from traps. With increasing Nb concentration, the contribution of bulk charge transport mechanisms like electron trapping at Ti^{4+} sites (trap energy of 1 eV) to internal field increases, leading to occurrence of higher magnitude of imprint in PZT films.

4.3 | The stability of imprinted state in Mn and Nb doped PZT films

The stability of the imprinted state in the PMZT and PNZT films induced by poling the samples at 25-200°C was examined under high field. P-E hysteresis measurements were made on equivalent electrodes immediately after poling at 150°C and 1, 2, 4, 6, or 24 hours after the poling. Figure 12 exhibits the change in the magnitude of imprint in PMZT films as a function of time after poling. The samples were aged at 180°C to increase the aging rate, as it was very slow at room temperature. The magnitude of imprint was calculated from the shifts along the electric field axis in P-E hysteresis loops. As shown in Figure 12, the stability of the imprint with aging time at 180°C showed significant differences for Mn and Nb doped PZT films. For Mn doped PZT films, the magnitude of imprint slightly decreased after 24 hours, indicating that voltage shift is mostly conserved. For Nb doped PZT films, on the other hand, the imprint gradually decreased with time and completely disappeared after 24 hours at 180°C. The difference in stability of imprint is consistent with the hypothesis that the mechanism for inducing imprint in Mn and Nb doped PZT films differs. The physical origin of imprint in Mn doped PZT films arises from alignment of defect dipoles like $(Mn''_{Ti} - V_O^{\cdot\cdot})^x$, $(Mn'_{Ti} - V_O^{\cdot\cdot})'$ along the polarization direction. A strong defect association between singly ionized manganese ions Mn'_{Ti} and $V_O^{\cdot\cdot}$ due to Jahn-Teller distortion[48] significantly improves the stability of these defect complexes upon thermal aging at 180°C, and hence the poled state is mostly preserved. For Nb doped PZT films, on the other hand, the induced imprint is mostly due to injection or/and trapping of electronic charges rather than movement of oxygen vacancies. These trapped charges tend to relax upon thermal aging, leading to reduction of imprint in Nb doped PZT films on aging at 180°C.

As expected, the internal field improves the stability of the remanent piezoelectric properties. As shown in Figure 13, the imprint in Mn doped PZT films leads to dramatic reductions
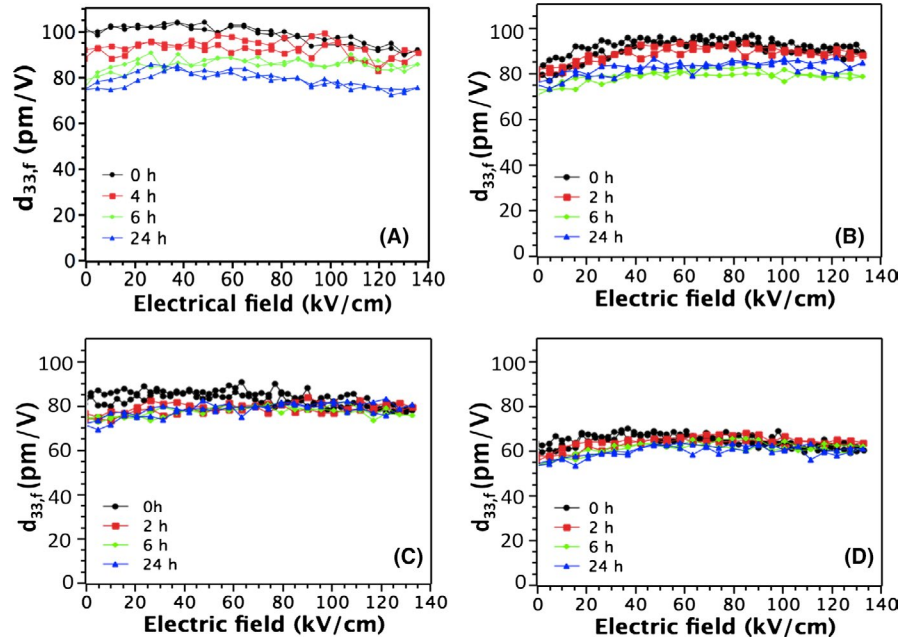
FIGURE 13 Time stability of $d_{33,f}$ in (A) 0.5, (B) 1, (C) 2, (D) 4% Mn doped PZT films measured at room temperature following aging at 180°C [Colour figure can be viewed at wileyonlinelibrary.com]
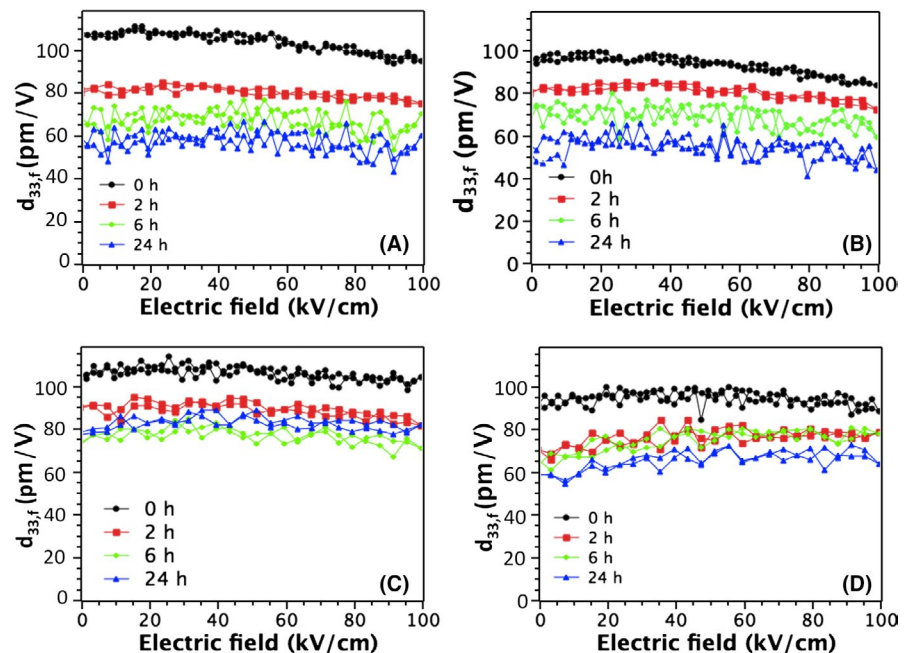

FIGURE 14 Time stability of $d_{33,f}$ in (A) 0.5, (B) 1, (C) 2, (D) 4% Nb doped PZT film measured at room temperature following aging at 180°C [Colour figure can be viewed at wileyonlinelibrary.com]

in aging. The 180°C aging rate of 0.5% Mn doped PZT film is 6.8%/decade and this rate decreases to 4.4, 3.1, and 2.3%/decade for 1, 2, and 4% Mn doped PZT films, respectively. The reduction in high temperature aging rates is attributed to improved stability of the poled state.

In contrast, PNZT films showed significantly larger high temperature $d_{33,f}$ aging rates, demonstrating that the fully poled state was not retained with time (Figure 14). 0.5%, 1%, 2%, and 4% Nb doped PZT films had 180°C aging rates of 13.6%, 13.1%, 7.6%, and 6.8%/decade, respectively. The sharp decrease in the piezoelectric properties is the result of polarization loss due to backswitching of the ferroelectric domains.[7] Imprint reduces

aging more effectively in acceptor doped PZT films, with respect to donor doped ones, following a high temperature poling step.

5 | CONCLUSIONS

The development of internal field and its effect on remanent piezoelectric properties and aging were studied in Mn and Nb doped PZT (Zr/Ti: 52/48) thin films. Crack free, homogenous, and smooth films were obtained by chemical solution deposition. Both Mn and Nb doped films are approximately randomly oriented.

Both Mn and Nb doped PZT films develop imprint on poling. Nevertheless, for all dopant levels and poling temperatures, the magnitude of imprint was found to be higher in PMZT films; the internal field changed from 3 to 32 kV/cm and 0.5 to 18 kV/cm for PMZT and PNZT films, respectively, for poling at temperatures from 25°C to 200°C. The enhanced internal field in the PMZT films was attributed to higher oxygen vacancy concentrations on Mn doping. In PMZT films, the E_a for the development of imprint varied from 0.5 ± 0.06 to 0.8 ± 0.1 eV as a function of [Mn], suggesting that the movement of oxygen vacancies and orientation of defect dipoles are responsible for the imprint developed. Higher E_a (0.8 ± 0.1-1.2 ± 0.2 eV) were characteristic of the development of imprint in PNZT films. Thermionic emission of electrons and subsequent electron trapping by Ti^{4+} trap sites are likely to be origin for the occurrence of imprint in PNZT films. The contribution of charge trapping processes to the internal field increases at higher Nb levels, leading to a reduction in the E_a for imprint.

The presence of an internal field improves the $d_{33,f}$ in both PMZT and PNZT films. However, the enhancement in $d_{33,f}$ due to imprint is more obvious in PMZT films, where larger internal fields can be introduced during poling. It was also found that imprint reduces aging more effectively in Mn doped PZT films, relative to Nb doped ones, following a high temperature poling step. This is attributed to enhanced stability of the poled state in acceptor doped films due to a strong defect association between singly ionized manganese ions Mn'_{Ti} and $V_O^{\cdot\cdot}$ (Jahn-Teller distortion). The higher aging rate in PNZT films is associated with loss of the internal field due to relaxation of trapped charges during aging.

ORCID

Betul Akkopru-Akgun (iD) https://orcid.org/0000-0003-3214-9603

Susan Trolier-McKinstry (iD) https://orcid.org/0000-0002-7267-9281

REFERENCES

1. Trolier-McKinstry S, Muralt P. Thin film piezoelectrics for MEMS: special issue on electroceramics in micro-electro-mechanical systems. J Electroceram. 2004;12:7–17.

2. Muralt P, Kholkin A, Kohli M, Maeder T. Piezoelectric actuation of PZT thin-film diaphragms at static and resonant conditions. Sens Actuators A Phys. 1996;53:398–404.

3. Shepard JF Jr, Moses PJ, Trolier-McKinstry S. The wafer flexure technique for the determination of the transverse piezoelectric coefficient (d_{31}) of PZT thin films. Sens Actuators A Phys. 1998;71C:133–8.

4. Damjanovic D. Ferroelectric, dielectric and piezoelectric properties of ferroelectric thin films and ceramics. Rep Prog Phys. 1998;61:1267–324.

5. Setter N, Damjanovic D, Eng L, Fox G, Gevorgian S, Hong S, et al. Ferroelectric thin films: review of materials, properties, and applications. J Appl Phys. 2006;100:051606–46.

6. Schulze WA, Ogino K. Review of literature on aging of dielectrics. Ferroelectrics. 1988;87:361–77.

7. Polcawich RG, Trolier-McKinstry S. Piezoelectric and dielectric reliability of lead zirconate titanate thin films. J Mater Res. 2000;15:2505–13.

8. Kholkin AL, Tagantsev AK, Colla EL, Taylor DV, Setter N. Piezoelectric and dielectric aging in Pb(Zr, Ti)O3 films and bulk ceramics. Integr Ferroelectr. 1997;15:317–24.

9. Drougard ME, Young DR. Domain clamping effect in barium titanate single crystals. Phys Rev. 1954;94:1561–4.

10. Postnikov VS, Pavlov VS, Turkov SK. Internal friction in ferroelectrics due to interaction of domain boundaries and point defects. J Phys Chem Sol. 1970;31:1785–91.

11. Takahashi M. Space charge effect in lead zirconate titanate ceramics caused by the addition of impurities. Jpn J Appl Phys. 1970;9:1236–46.

12. Robels U, Arlt G. Domain wall clamping in ferroelectrics by orientation of defects. J Appl Phys. 1993;73:3454–60.

13. Morozov MI, Damjanovic D. Charge migration in Pb(Zr, Ti)O3 ceramics and its relation to ageing, hardening, and softening. J Appl Phys. 2010;107:034106-1-10.

14. Carl K, Hardtl KH. Electrical after-effects in Pb(Zr, Ti)O3 ceramics. Ferroelectrics. 1978;17:473–86.

15. Jonker GH. Nature of aging in ferroelectric ceramics. J Am Ceram Soc. 1972;55:57–8.

16. McQuarrie MC, Buessem WR. The aging effect in barium titanate. Ceram Bull. 1955;34:402–6.

17. Thomann H. Stabilization effects in piezoelectric lead titanate zirconate ceramics. Ferroelectrics. 1972;4:141–6.

18. Arlt G, Neumann H. Internal bias in ferroelectric ceramics: origin and time dependence. Ferroelectrics. 1988;87:109–20.

19. Glaum J, Genenko YA, Kungl H, Schmitt LA, Granzow T. De-aging of Fe-doped lead-zirconate-titanate ceramics by electric field cycling: 180°- vs. non-180° domain wall processes. J Appl Phys. 2012;112:034103-1-9.

20. Smyth DM. Defect structure in perovskite titanates. Curr Opin Solid State Mater Sci. 1996;1:692–7.

21. Smyth DM. Ionic transport in ferroelectrics. Ferroelectrics. 1994;151:115–24.

22. Raymond MV, Smyth DM. Defects and charge transport in perovskite ferroelectrics. J Phys Chem Solids. 1996;57:1507–11.

23. Newnham RE. Review article: electroceramics. Rep Prog Phys. 1989;52:123–56.

24. Jaffe B, Cook WR, Jaffe H. Piezoelectric ceramics. New York, NY: Academic Press; 1971: p. 139.

25. Robertson J, Warren WL, Tuttle BA, Dimos D, Smyth DM. Shallow Pb^{3+} hole traps in lead zirconate titanate ferroelectrics. Appl Phys Lett. 2012;63:1519–21.

26. Scholz JR. Aging rates in PZT ferroelectrics with mixed acceptor-donor dopants. University Park, PA: Penn State University; 2009: p. 55.

27. Warren WL, Dimos D, Pike GE, Tuttle BA, Raymond MV. Voltage shifts and imprint in ferroelectric capacitors. Appl Phys Lett. 1995;67:866–8.

28. Dimos D, Warren WL, Sinclair MB, Tuttle BA, Schwartz RW. Photoinduced hysteresis changes and optical storage in (Pb, La)(Zr, Ti)O3 thin films and ceramics. J Appl Phys. 1994;76:4305–15.

29. Warren WL, Dimos D, Pike GE, Vanheusden K, Ramesh R. Alignment of defect dipoles in polycrystalline ferroelectrics. Appl Phys Lett. 1995;67:1689–91.

30. Kholkin AL, Setter N. Photoinduced poling of lead titanate zirconate thin films. Appl Phys Lett. 1997;71:2854–6.

31. Grossmann M, Lohse O, Bolten D, Boettger U, Schneller T. The interface screening model as origin of imprint in $PbZr_xTi_{1-x}O_3$ thin films. I. dopant, illumination, and bias dependence. J Appl Phys. 2002;92:2680–7.

32. Koval V, Viola G, Tan Y. Ferroelectric materials: synthesis and characterization: biasing effects in ferroic materials. Rijeka, Croatia: Intech; 2015: pp. 205–45.

33. Boettger U, Braeuhaus D, Waser R. The influence of non-ferroelectric interface layers and inclusions on the imprint behavior of ferroelectric thin film capacitors. Sixteenth IEEE International Symposium on the Applications of Ferroelectrics. 2007: 32–4.

34. Takahashi S. Effects of impurity doping in lead zirconate-titanate ceramics. Ferroelectrics. 1982;4:143–56.

35. Zhang Q, Whatmore RW. Improved ferroelectric and pyroelectric properties in Mn-doped lead zirconate titanate thin films. J Appl Phys. 2003;94:5228–33.

36. Wolf RA, Trolier-McKinstry S. Temperature dependence of the piezoelectric response in lead zirconate titanate films. J Appl Phys. 2004;95:1397–406.

37. Fujii I. Dielectric nonlinearity of ferroelectrics. University Park, PA: Penn State University; 2010: p. 22.

38. Kurchania R, Milne SJ. Characterization of sol-gel $Pb(Zr_{0.53}Ti_{0.47})O_3$ films in the thickness range 0.25–10 μm. J Mater Res. 1998;14:1852–9.

39. Zhu W, Fujii I, Ren W, Trolier-McKinstry S. Influence of Mn doping on domain wall motion in $Pb(Zr_{0.52}Ti_{0.48})O_3$ films. J Appl Phys. 2011;109:064105-6.

40. Zhu W, Fujii I, Ren W, Trolier-McKinstry S. Domain wall motion in A and B site donor-doped $Pb(Zr_{0.52}Ti_{0.48})O_3$ Films. J Am Ceram Soc. 2012;95:2906–13.

41. Chan NH, Smyth DM. Defect chemistry of donor-doped BaTiO3. J Am Ceram Soc. 1984;67:285–8.

42. Warren WL, Tuttle BA, Dimos D, Pike GE, Al-Shareef HN, Ramesh R, et al. Voltage shifts and defect-dipoles in ferroelectric capacitors. Jpn J Appl Phys. 1996;35:1521–30.

43. Boukamp BA, Pham MTN, Blank DHA, Bouwmeester HJM. Ionic and electronic conductivity in lead-zirconate-titanate (PZT). Solid State Ionics. 2004;170:239–54.

44. Garten L. Residual ferroelectricity, piezoelectricity, and flexoelectricity on barium strontium titanate tunable dielectrics. University Park, PA: Penn State University; 2014: p. 152.

45. Grossmann M, Lohse O, Schneller T, Bolten D, Boettger U, Rodriguez Contreas J, et al. Imprint in ferroelectric Pb(Zr, Ti)O3 thin films with thin SrRuO3 layers at the electrodes. Integr Ferroelectr. 2001;37:205–14.

46. Carim AH, Tuttle BA, Doughty DH, Martinez SL. Microstructure of solution-processed lead zirconate titanate (PZT) thin films. J Am Ceram Soc. 1991;74:1455–8.

47. Tuttle BA, Headley TJ, Bunker BC, Schwartz RW, Zender TJ, Hernandez CL, et al. Microstructural evolution of $Pb(Zr, Ti)O_3$ thin films prepared by hybrid metallo-organic decomposition. J Mater Res. 1992;7:1876–82.

48. Ng YS, Alexander SM. Structural studies of manganese stabilised lead-zirconate-titanate. Ferroelectrics. 1983;51:81–6.